Valence-state mixing and separation in $SmBaFe_2O_{5+w}$

J. Lindén
Department of Physics, Åbo Akademi, FIN-20500 Turku, Finland

P. Karen and A. Kjekshus
Department of Chemistry, University of Oslo, N-0315 Oslo, Norway

J. Miettinen* and T. Pietari
Department of Technical Physics, Helsinki University of Technology, FIN-02015 Espoo, Finland

M. Karppinen
Laboratory of Inorganic and Analytical Chemistry, Helsinki University of Technology, FIN-02150 Espoo, Finland

(Received 23 June 1999)

A mixed-valence state, formally denoted as $Fe^{2.5+}$, is observed in the 300 K Mössbauer spectra of the most reduced samples of $SmBaFe_2O_{5+w}$. Upon cooling below the Verwey-type transition temperature ($T_V \approx 200$ K), the component assigned to $Fe^{2.5+}$ separates into a high-spin Fe^{3+} state and an Fe^{2+} state with an unusually low internal field. The separation of the mixed-valence state at T_V is also confirmed by magnetic susceptibility measurements and differential scanning calorimetry. A model is proposed which accounts for the variation of the amount of the mixed-valence state with the oxygen content parameter *w*.
[S0163-1829(99)00446-4]

I. INTRODUCTION

The occurrence of valence-state mixing, separation and (spatial) ordering has in recent years received considerable attention. Such phenomena have, since the first discovery of a partial valence-state mixing-separation transition in Fe_3O_4 (often named the Verwey transition, see, e.g., Ref. 1) been found in different types of materials (ranging from alloys to ionic substances, encompassing metallic conductors, semiconductors, and ionic conductors) and various elements (hitherto limited to transition metals and rare earths).

Mixed-valence states (or scientifically more descriptive: spontaneous interconfiguration fluctuations) have, e.g., been reported in ternary rare-earth phases,[2–4] where solid solubility was used to adjust the formal valence state of the rare-earth component to a value between 2+ and 3+. At low temperatures both valence states can be observed experimentally, e.g., by ^{151}Eu Mössbauer spectroscopy.[3] At more elevated temperatures the two valence states are no longer distinguishable and instead an intermediate valence state is observed. In $La_{1-x}Eu_xRh_2$ the mixing is attributed to electrons fluctuating between the conduction band and the localized $4f$ levels of the Eu atoms with a frequency of the order of 10^{13} Hz.[3] A mixed-valence state of iron has been observed in ternary oxides, such as $Fe(Nb_{1-x}W_x)O_4$.[5,6] Again the mixed-valence state is achieved by choosing a suitable mixture of Nb^{5+} and W^{6+}, thus forcing iron to adjust its valence to a value between 2+ and 3+. A somewhat different scenario is reported for Fe_3O_4, in which a mixed-valence state for some of the iron atoms is observed at room temperature.[1] The atoms in Fe_3O_4 occupy two different crystallographic sites (one with a tetrahedral environment the other with an octahedral). The tetrahedral site is populated by Fe^{3+} only, whereas the octahedral site contains an equal amount of Fe^{2+} and Fe^{3+}. Above a critical temperature [in the following designated Verwey transition temperature; $T_V \approx 120$ K (Ref. 1)] the two Fe valence states in the octahedral site become indistinguishable, due to a fast electron exchange between Fe^{2+} and Fe^{3+} and the site appears as being populated by $Fe^{2.5+}$. Other reported examples of mixed iron valence concern also higher valence states Fe^{3+}, Fe^{4+}, and Fe^{5+}, as exemplified by $CaFeO_3$,[7] $SrFeO_3$,[8] and $PrSr_2Fe_3O_{9-\delta}$ (Ref. 9) from the perovskite family.

In this paper we present results on the $SmBaFe_2O_{5+w}$ double perovskite[10] where the oxidation state of iron is varied from 2.52 to 3.15. The double-perovskite arrangement (prototype $YBaFeCuO_5$) (Ref. 11) is the first member of a series of uniaxially ordered perovskite-type structures which also include, e.g., $YBa_2Cu_3O_7$ and $YBa_2Fe_3O_8$.

II. EXPERIMENTAL

Syntheses. The bulk $SmBaFe_2O_{5+w}$ material was synthesized[10,12] from a citrate-based nanoprecursor, starting with iron lumps (99.95%, Koch-Light), Sm_2O_3 (99%, Molycorp), and $BaCO_3$ (0.1% Sr, Merck). The precursor was calcined at 900 °C in a reducing atmosphere ($Ar/H_2 \approx 30$ by volume). According to powder x-ray diffraction (PXD), the brown-colored calcinate was practically single phase, with broad Bragg peaks. Subsequent sintering at 985 °C ($Ar/H_2 \approx 20$ by volume) gave compact samples with a silvery luster and sharp PXD Bragg peaks.

Oxygen content control. The content of oxygen in the double-perovskite phase was defined by the temperature and the partial pressure of oxygen in mixtures of argon, hydrogen, or oxygen (all 99.999%) and water vapor (wetting solution: ~45 wt. % H_3PO_4 of calibrated concentration and temperature) according to thermodynamic data.[13,14] After a

120 h equilibration at 985 or 1000 °C, the fully sintered samples were quenched into the dry (not wetted) gas of the same mixture (initial quenching rate 300 °C/min; except for samples from the interval $0.20<w<0.40$ which were quenched at least ten times faster, into a metal container filled with high purity Ar).

Oxygen content analyses. The oxygen content was determined by cerimetric titration, described in detail in Ref. 10. Each titration was performed in duplicate or triplicate.

Powder x-ray diffraction. The phase purity and unit-cell dimensions of all samples were evaluated from PXD data obtained with a Guinier-Hägg camera with Cu$K\alpha_1$ radiation and Si as an internal standard. The photographs were scanned by an LS-18 (Nicolet) film scanner with the SCANPI (Ref. 15) software.

Mössbauer spectroscopy. The Mössbauer absorbers were made by mixing 30 mg of the sample material with varnish and spreading it evenly on an Al foil. The sample covered an area of ~ 1.2 cm^2. The measurements were performed using an Amersham ^{57}Co: Rh (20 mCi, January 1995) source, between March 1998 and May 1999. Some of the low-temperature spectra were measured using an identical source, activated in November 1998. After changing the source it was confirmed that virtually identical spectra were obtained using either of the two sources. The Mössbauer spectra were recorded at fixed temperatures in the temperature range 5–300 K in transmission geometry using a maximum Doppler velocity of 15 mm/s. All spectra exhibited cooperative magnetic splitting. The spectra were fitted with the full Hamiltonian of combined electric and magnetic interactions. The following hyperfine parameters were included in the fit: the internal magnetic field experienced by the Fe nucleus (B), the chemical isomer shift relative to α-Fe (δ), the quadrupole coupling constant (eQV_{zz}), the resonance linewidths (Γ), and the relative intensities of the components (I). The following conditions and constraints were applied: (i) For each component a certain variation in the parameter B was allowed in order to simulate the fact that the internal fields have a certain spread due to, e.g., local distortions of the coordination polyhedra. A Gaussian distribution was assumed and its width (ΔB) was introduced as a fit parameter. (ii) The asymmetry parameter η and the angle θ between the direction of the magnetic and the electric quantization axes were omitted in most fittings (set equal to zero). (iii) All components were constrained to have equal line widths Γ. (iv) A small asymmetric quadrupole component, originating from traces of iron in the Be detector window and in the Al foil was kept fixed during the fits. These impurity defects cover less than $\sim 2\%$ of the spectral intensity obtained in the measurements.

Magnetic susceptibility. Magnetic susceptibility data were collected with an MPMS (magnetic properties measurement system; Quantum Design) apparatus. Measurements were performed upon heating (zero field cooled samples) between 5 and 300 K using a measurement field of 500 Oe and ~ 50 mg samples.

Differential scanning calorimetry (DSC). DSC data were obtained with a Mettler DSC 3000 system between 120 and 450 K using 20 to 50 mg samples. Aluminum containers were used as sample holders. CrAs was measured under same conditions, and its magnetic transition at 260 K was used as an enthalpy standard.[16]

TABLE I. $SmBaFe_2O_{5+w}$ samples; cerimetric oxygen content, unit-cell dimensions, and quenching partial pressure of oxygen ($t = 985$ °C). Standard deviations in round brackets.

$5+w$	a (Å)	b (Å)	c (Å)	$\log p_{O_2}$ (bar)
5.022(1)	3.9491(4)	3.9581(4)	7.6183(10)	−15.67(2)
5.036(2)	3.9470(4)	3.9565(4)	7.6222(13)	−15.04(4)
5.077(3)	3.9510(2)		7.6371(7)	−15.59(6)
5.091(1)	3.9511(4)		7.6374(6)	−14.49(1)
5.152(2)	3.9504(3)		7.6549(9)	−13.98(1)
5.202(1)	3.9494(2)		7.6651(7)	−14.03(2)
5.255(2)	3.9455(2)		7.6879(8)	−13.67(2)
5.300(2)	3.9466(4)		7.7023(12)	−13.47(1)
5.320(1)	3.9426(3)		7.7049(7)	−12.44(4)[a]
5.349(1)	3.9435(5)		7.7151(12)	−12.05(1)[a]
5.414(1)	3.9430(4)		7.7314(15)	−12.57(3)
5.498(1)	3.9383(3)		7.7532(8)	−4 [Ar]
5.527(2)	3.9373(3)		7.7580(7)	−2.87(3)
5.582(2)	3.9376(4)		7.7659(14)	−1.56(3)
5.646(2)	3.9272(6)		7.8237(28)	−0 [O_2]

[a]At 1000 °C.

III. RESULTS

According to PXD, only the double-perovskite-type phase could be identified in the samples with $w<0.30$ after the quenching. Samples with higher oxygen content contained some 3 wt. % of $SmFeO_3$. As indicated by synchrotron x-ray diffraction,[10] the fully stoichiometric sample ($w=0.50$) may contain a small portion of a fully disordered cubic phase (Ba,Sm)FeO_3, completely overlapping with reflections from the main phase in the conventional PXD pattern. The synthesis conditions, and characterization results are listed in Table I. The crystal structure (Fig. 1; see Ref. 10) is tetragonal ($P4/mmm$) except for the samples in the most reduced region where a slight orthorhombic distortion is observed. The entire span in the oxygen content examined in this study ($0.022 \leqslant w \leqslant 0.646$) concerns only one site in the crystal structure, and this site is designated as O(4). The structural representation in Fig. 1 shows that the Fe atom has either a square-pyramidal or an octahedral oxygen coordination, depending on whether the O(4) site is locally occupied or not. The amount of five- and six-coordinated Fe is therefore uniquely determined by the value of the composition parameter w. Moreover, assuming that the valence states of Sm^{3+}, Ba^{2+}, and O^{2-} are fixed (and neglecting any degree of Fe^{3+} disproportionation) the amounts of trivalent and divalent or tetravalent iron will be uniquely determined by the value of w. In the most reduced sample ($w=0.022$; attempts to prepare $w=0$ led to decomposition) 47.8% Fe^{2+} and 52.2% Fe^{3+} is needed in order to achieve charge neutrality, while in the most oxidized sample ($w=0.646$) the corresponding figures are 85.4% Fe^{3+} and 14.6% Fe^{4+}. Whereas Fe^{2+} and Fe^{4+} are unambiguously associated with CN5 and CN6, respectively, Fe^{3+} may take either cordination.

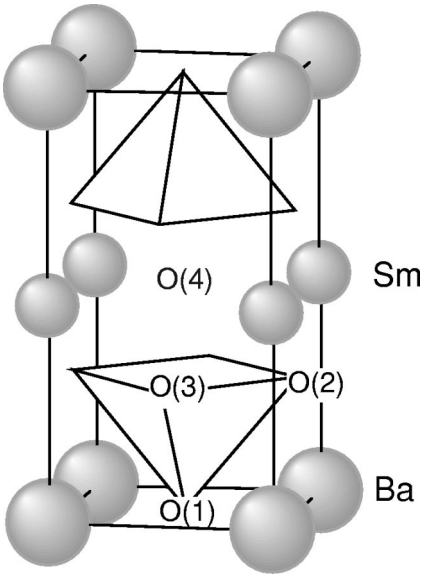

FIG. 1. The $SmBaFe_2O_{5+w}$ unit cell with the coordination square pyramids around Fe. The added (w) oxygens appear at the O(4) site.

A. Mössbauer spectra at 300 K

Figure 2 gives room-temperature Mössbauer spectra for selected $SmBaFe_2O_{5+w}$ samples, showing also the spectral components used in the fits. All spectra were fitted using magnetic sextets, reflecting the antiferromagnetic (AF) ordering. No paramagnetic components, except for the detector impurity, were observed. Figure 3 gives the isomer shifts extracted from the fits and the assigned valence and spin states. Judging from the large splitting between the resonance lines, most components belong clearly to high-spin states, i.e., $S=2$ for Fe^{2+} and Fe^{4+}, and $S=5/2$ for Fe^{3+}. Confirmed assignments are obtained with the help of the other fit parameters as described below.

A clear-cut situation occurs for the composition with trivalent iron ($w=0.5$). Here the spectrum (actual composition $w=0.498$) has two components corresponding to five- and six-coordinated iron: ${}^{CN5}_{AF}Fe^{3+}_{S5/2}$ and ${}^{CN6}_{AF}Fe^{3+}_{S5/2}$, present in equal amounts. The same two components were also identified in the recent studies[18,19] of the $Y(Ba,La)(Cu_{0.5+x}Fe_{0.5-x})_2O_{5+w}$ double perovskites with trivalent iron. When w decreases below 0.5, signatures of increasing amounts of Fe^{2+} are found. In addition to this, a new component appears, which at $w=0.022$ assumes 82% of the spectral intensity (Fig. 4). Neither divalent nor trivalent iron can account for such a large intensity fraction (as well as for other Mössbauer parameters for this component), and this suggests a mixed-valence state $Fe^{2.5+}$.

Upon increasing w from zero, the intensity of this mixed-valence component ${}^{CN5}_{AF}Fe^{2.5+}_{IS}$ (IS denotes intermediate spin state) rapidly decreases, giving rise to corresponding amounts of integer-valence states in square-pyramidal coordinations; ${}^{CN5}_{AF}Fe^{2+}_{S2}$ and ${}^{CN5}_{AF}Fe^{3+}_{S5/2}$. A certain broadening of the resonance lines in the 300 K Mössbauer spectra is observed for compositions around $w=0.30$. In this region, an additional component appears in the spectrum and is assigned to a ${}^{CN5}_{AF}Fe^{2+}_{US}$ state (US denotes unidentified spin state), based mainly on the isomer shift values.

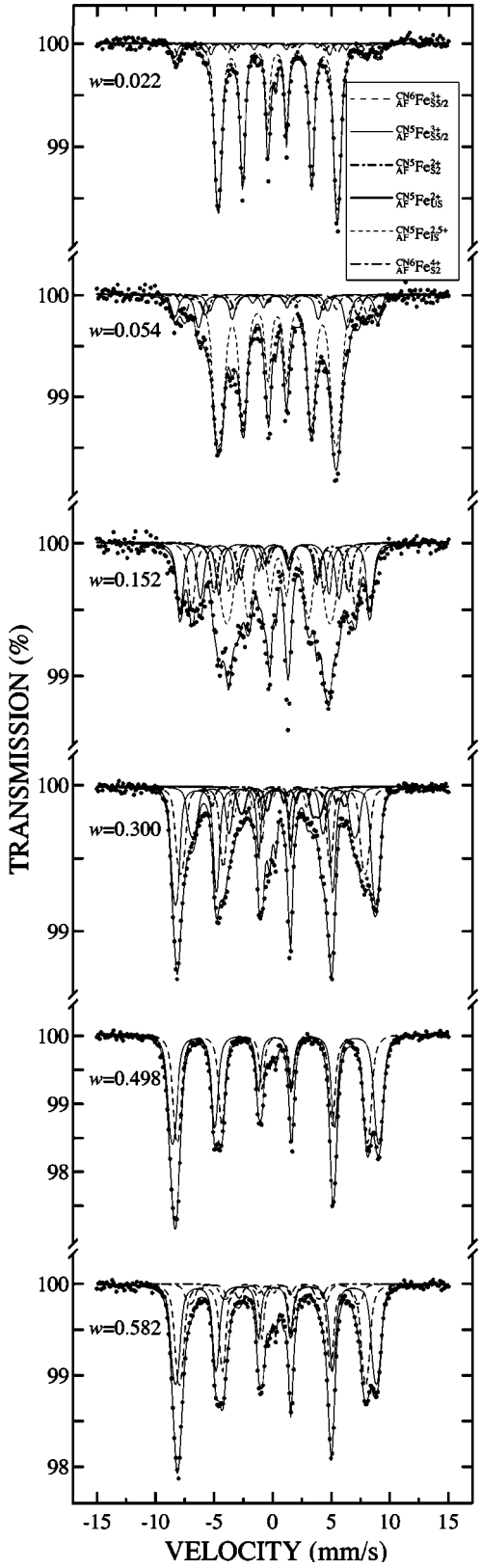

FIG. 2. Fitted ^{57}Fe Mössbauer spectra of selected $SmBaFe_2O_{5+w}$ samples recorded at 300 K. Compositions and component assignments are presented on the illustrations.

The trivalent iron state ${}^{CN5}_{AF}Fe^{3+}_{S5/2}$ for $w<0.5$ is accompanied by a satellite, appearing as a non-Gaussian tail in the distribution of the hyperfine parameters of the main component. A similar satellite is also seen for the oxidized samples

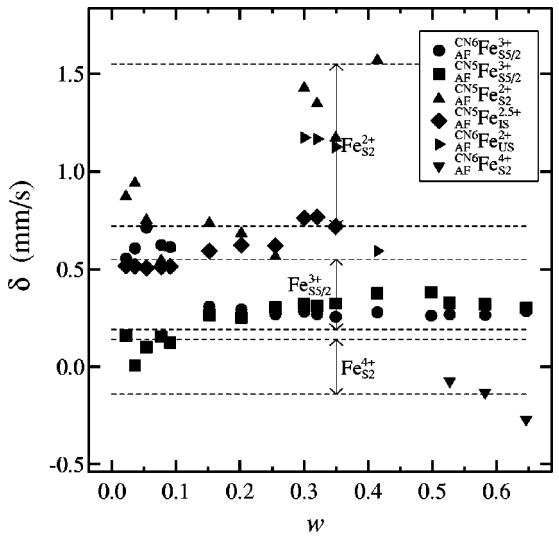

FIG. 3. Isomer shifts relative to α-Fe for identified spectral components of the 300 K Mössbauer spectra of $SmBaFe_2O_{5+w}$. Standard deviations do not exceed the size of symbols. Usual ranges of isomer shifts according to Ref. 17 are indicated. In this and following illustrations the component labels are shown in the legend.

($w>0.5$), here accompanying the $^{CN6}_{AF}Fe^{3+}_{S5/2}$ component. The satellites differ from their parent components essentially only in the value of their internal fields and are reported also in Mössbauer studies of other RBa $(Cu,Fe)_2O_5$ phases.[18,20] In Fig. 2 both the parent component and its satellite are drawn with the same line type, and their intensities are added in Fig. 4. In the illustrations displaying the hyperfine parameters the satellites are omitted for clarity. At 77 K the satellites are no longer observed, and single components with expected intensities are obtained (Sec. III B). One tetravalent iron state is identified in the oxidized samples, assigned to a fully occupied octahedral coordination of high-spin iron ($^{CN6}_{AF}Fe^{4+}_{S2}$).

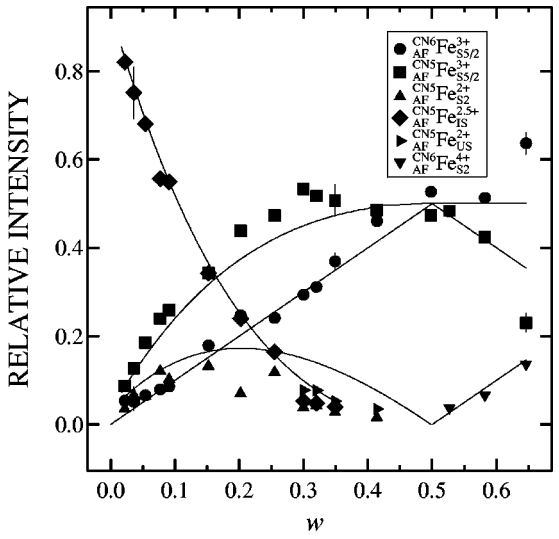

FIG. 4. Mössbauer intensities of $SmBaFe_2O_{5+w}$ at 300 K. Standard deviations that exceed the size of symbols are marked with bars. Lines represent ideal case for the valence states and coordinations concerned.

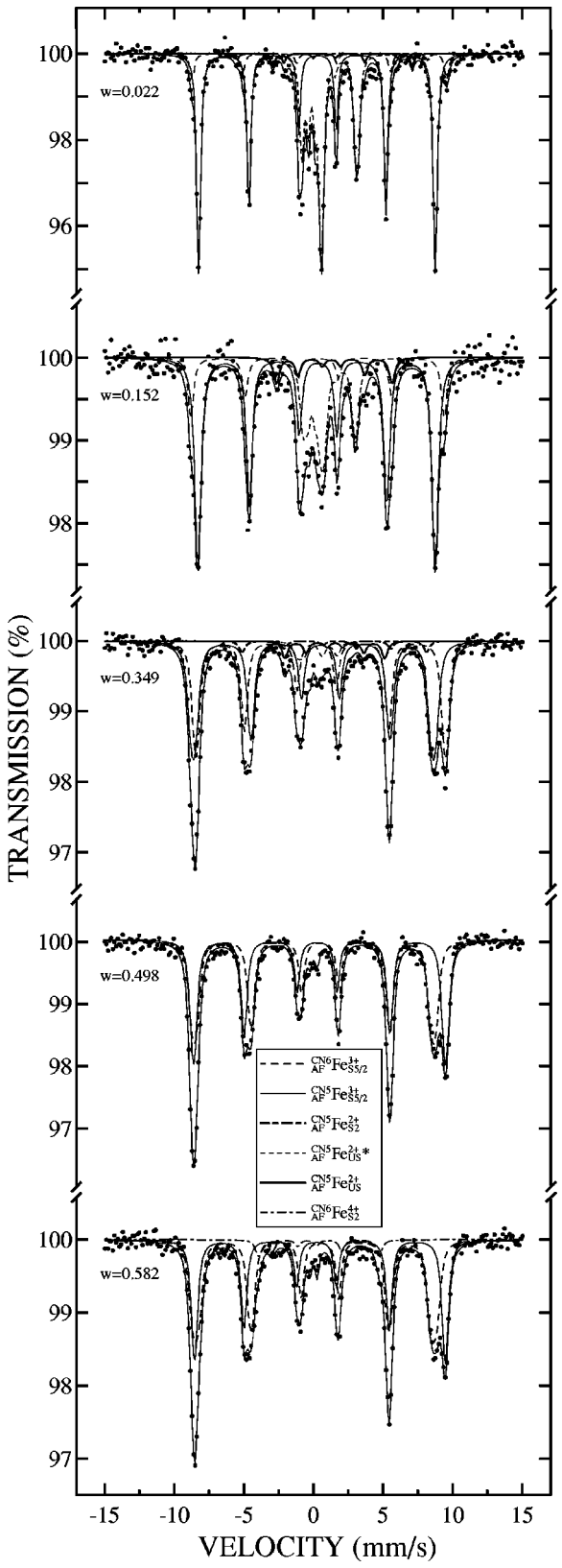

FIG. 5. Mössbauer spectra of $SmBaFe_2O_{5+w}$ samples recorded at 77 K. Component assignments are presented on the illustration.

B. Low-temperature Mössbauer spectra

Figure 5 shows selected Mössbauer spectra of $SmBaFe_2O_{5+w}$ recorded at 77 K (the sample with $w=0.022$ was also measured at 5 K giving an essentially iden-

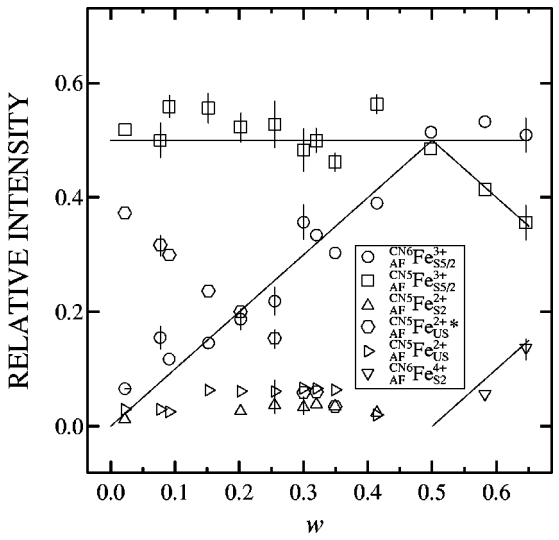

FIG. 6. Mössbauer intensities of $SmBaFe_2O_{5+w}$ at 77 K. Standard deviations that exceed the size of symbols are marked with bars. Lines represent the ideal case for the components concerned.

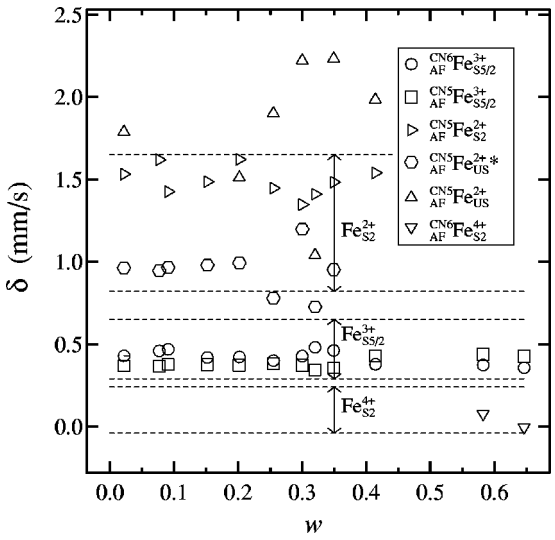

FIG. 8. Isomer shifts of the Mössbauer components of $SmBaFe_2O_{5+w}$ at 77 K. Usual ranges of isomer shifts are indicated (Ref. 17; 0.10 mm/s is added as an estimated temperature correction in the second-order Doppler shift). Standard deviations do not exceed the size of symbols.

tical spectrum). The mixed-valence component (see Fig. 2) is no longer present. Instead, the 77 K spectra for the most reduced samples are dominated by two intense components (Fig. 6) with internal fields of ~53 and ~8 T (Fig. 7). The isomer shifts (Fig. 8) are 0.36 and 0.95 mm/s, respectively, and this suggests that the 53 T component represents a trivalent high-spin state ($^{CN5}_{AF}Fe^{3+}_{S5/2}$) whereas the 8 T component belongs to a divalent state. The extremely low field suggests either low-spin $^{CN5}_{AF}Fe^{2+}_{S1}$, or high-spin $^{CN5}_{AF}Fe^{2+}_{S2}$, the latter subjected to a very strong transferred hyperfine field of opposite sign. This component is hereafter denoted as $^{CN5}_{AF}Fe^{2+}_{US}$*.

In addition to the two strong components, three weaker components are discerned in the Mössbauer spectra of the most reduced samples at 77 K. One has an internal field of ~55 T, an isomer shift of 0.45 mm/s, and intensity (Fig. 6) closely following the structural amount of octahedrally coordinated iron. This component is therefore assigned to $^{CN6}_{AF}Fe^{3+}_{S5/2}$. It is noteworthy that a crossover in internal field values between this and the 53 T component occurs around $w=0.37$ (Fig. 7), reflected also in the quadrupole coupling constants (*vide infra*). The second weak component has an internal field of ~40 T and an isomer shift of ~1.2 mm/s, which points at a high-spin $^{CN5}_{AF}Fe^{2+}_{S2}$ state. The third weak component is the $^{CN5}_{AF}Fe^{2+}_{US}$ state (with $B\approx 22$ T) seen already at 300 K, however, at 77 K occurring across the whole range $0<w<0.5$.

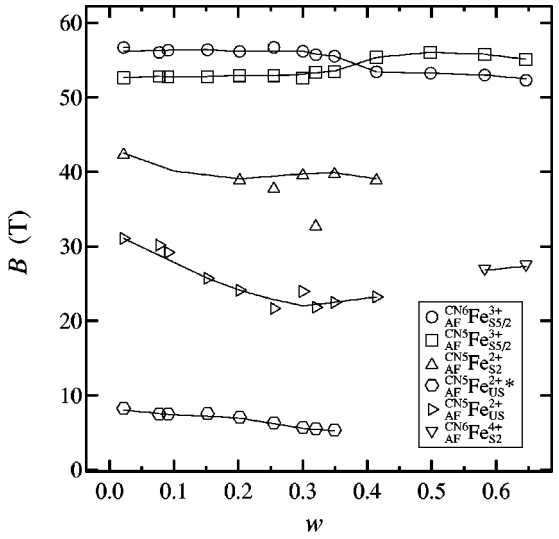

FIG. 7. Internal magnetic fields of the Mössbauer components of $SmBaFe_2O_{5+w}$ at 77 K. Standard deviations do not exceed the size of symbols. Lines are drawn as guides for the eye.

When the oxygen content is increased from the most reduced compositions, the intensity of the divalent daughter component ($^{CN5}_{AF}Fe^{2+}_{US}$*) decreases in favor of $^{CN6}_{AF}Fe^{3+}_{S5/2}$ whereas the intensities of the two weak divalent components do not vary appreciably up to w around 0.35, above which their intensity decreases to disappear before the composition $w=0.5$ is reached. For even more oxidized samples the tetravalent component appears in spectra which are similar to those at 300 K, but have somewhat stronger internal fields and narrower linewidths, as expected for low temperature data.

C. Compositional balance from assigned states

The assignment of the valence states has been checked by accounting the component intensities (Figs. 4 and 6) for the divalent, mixed-valent, trivalent, and tetravalent iron states into an average iron valence. The comparison with the cerimetric Fe valences in Fig. 9 shows very good agreement. A corroboration of the assigned coordination states is also obtained by calculating the amount of octahedrally coordinated iron from the component intensities of the Mössbauer spectra. The results presented in Fig. 10 agree well with the conditions dictated by the stoichiometry and the crystal structure.

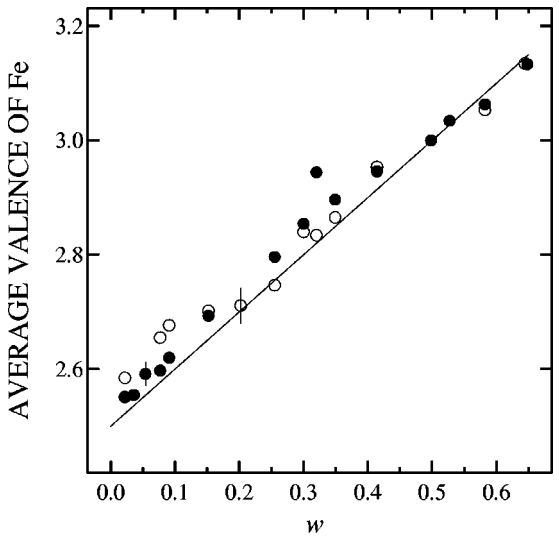

FIG. 9. Average Fe valence as obtained from intensities of Mössbauer spectra (points) and as defined by the cerimetric value of w for $SmBaFe_2O_{5+w}$ (line). Filled and open circles denote 300 and 77 K data, respectively. Standard deviations that exceed the size of symbols are marked with bars.

D. Valence-state mixing and separation

We will now present further evidence for the concept of two valence states merging to produce the mixed $^{CN5}_{AF}Fe^{2.5+}_{IS}$ state. At 77 K, the mixed-valence state has separated into the 8 T $^{CN5}_{AF}Fe^{2+}_{US}$* and 53 T $^{CN5}_{AF}Fe^{3+}_{S5/2}$ components (Fig. 6). By taking the arithmetic mean of the saturation fields for the sample with $w=0.022$ as an example, one gets $(53+8)/2$ T$=30.5$ T, which compares well with the $\sim$31 T maximum field of the $^{CN5}_{AF}Fe^{2.5+}_{IS}$ component for the mixed-valence state (Fig. 11). Furthermore, taking the average of the corresponding isomer shift values one gets $(0.36+0.95)/2$ mm/s which, after a correction for an estimated second-order Doppler shift of -0.10 mm/s,[17] gives 0.56 mm/s as a 300 K value. This is remarkably close to the isomer shift value of 0.52 mm/s obtained for the $^{CN5}_{AF}Fe^{2.5+}_{IS}$ component.

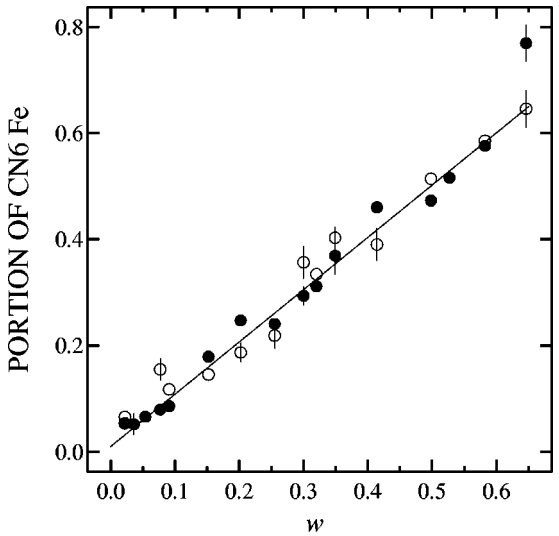

FIG. 10. Portion of ^{CN6}Fe as obtained from Mössbauer data (points) and as defined by the cerimetric value of w for $SmBaFe_2O_{5+w}$ (line). Filled and open circles denote 300 and 77 K data, respectively. Standard deviations that exceed the size of symbols are marked with bars.

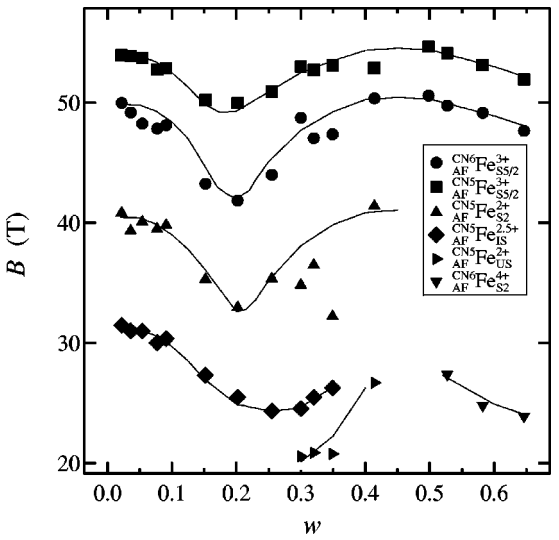

FIG. 11. Internal magnetic fields of the Mössbauer components of $SmBaFe_2O_{5+w}$ at 300 K. Lines are drawn as guides for the eye. Standard deviations do not exceed the size of symbols.

The quadrupole coupling constant (eQV_{zz}), which roughly measures the asymmetry in the charge distribution around the Mössbauer nuclei, lies between -0.17 and 0.13 mm/s at 300 K for $^{CN5}_{AF}Fe^{2.5+}_{IS}$ when the mixed-valence component is strong enough to guarantee accuracy (Fig. 12). At 77 K, it has separated into ~ -0.1 mm/s for Fe^{3+} and $\sim$3.6 mm/s for Fe^{2+} (Fig. 13). The average of these two values is $\sim$1.8 mm/s, which differs immensely from what is observed in the actual mixed-valence state, suggesting a (coordination) symmetry change, e.g., a charge-ordering transition. Another explanation involves the possible transferred hyperfine field (Sec. III B) which, in addition to that it would carry the large spin density to diminish the field to $\sim$8 T,

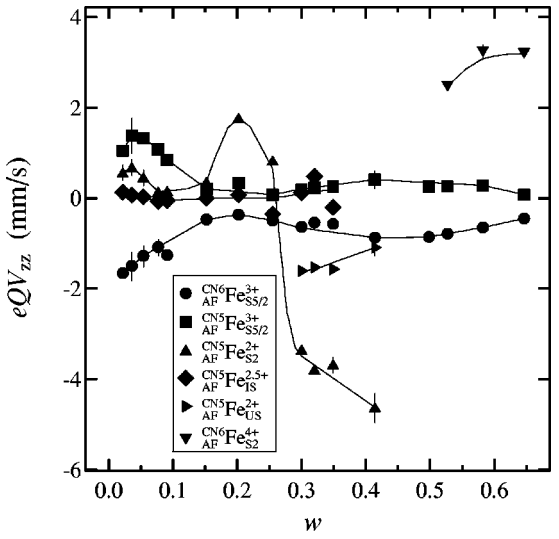

FIG. 12. Qudarupole coupling constants of the Mössbauer components of $SmBaFe_2O_{5+w}$ at 300 K. Lines are drawn as guides for the eye. Standard deviations that exceed the size of symbols are marked with bars.

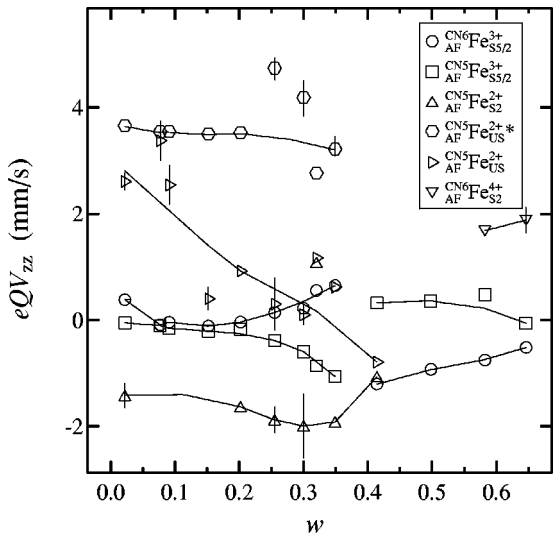

FIG. 13. Qudarupole coupling constants of the Mössbauer components of $SmBaFe_2O_{5+w}$ at 77 K. Lines are drawn as guides for the eye. Standard deviations that exceed the size of symbols are marked with bars.

also would introduce the charge distribution around the Fe^{2+} site that seems to be manifested in the large value for eQV_{zz}.

Symmetry considerations dictate that a regular square-pyramidal coordination of an ion located at the center of gravity has $eQV_{zz} \approx 0$ mm/s, and this is the case for the trivalent $^{CN5}_{AF}Fe^{3+}_{S5/2}$ component at 77 K with high internal field (53 T). Its divalent twin has a low field (8 T), but eQV_{zz} is large. Owing to this situation, the magnetic field vector and the main component of the electric field gradient (V_{zz}) cause line splitting of a comparable magnitude for this component, and are hence well suited for refinement of their mutual orientations. Consequently the implicit assumption that the angle θ between the two vectors is zero can be tested using this 8 T Mössbauer component. (The other components have either too weak intensities or too small eQV_{zz} to enable fitting of θ.) A trial release of this angle as a variable gave $\theta = 0$ within the fitting error. Since the symmetry of the iron coordination polyhedra in this crystal structure defines V_{zz} parallel to c, the result indicates that the AF-ordered spins are more or less parallel with the crystallographic c axis. This is different from the situation in $YBaFeCuO_5$ and $YBa_2Fe_3O_{8+w}$, where neutron diffraction locates the spins in the a,b plane.[21,22] The asymmetry parameter for the 8 T component is refined to ~ 0.7. Interestingly, no difference is seen between the tetragonal and orthorhombic samples, illustrating that the quadrupole interaction of the 8 T component is insensitive to such minor lattice deformations.

The temperature T_V (where the $Fe^{2.5+}$ mixed-valence state disappears on cooling and appears on heating) can be established from a series of Mössbauer spectra recorded at several temperatures around the expected transition. An example is shown in Fig. 14 for the sample with $w = 0.091$. Whereas the spectrum obtained at 190 K is practically identical with the (separated-valences) spectrum at 77 K, spectra collected at 200 and 240 K carry all the essential features of the (mixed-valence) 300 K spectrum. However, the linewidth (or rather ΔB) of particularly the $^{CN5}_{AF}Fe^{2.5+}_{IS}$ component increased strongly upon approaching the transition from above, and this seriously hampered the fitting procedure. The temperature T_V depends also on the oxygen content. As an example, charge-separated spectra were obtained up to 210 K for $w = 0.022$.

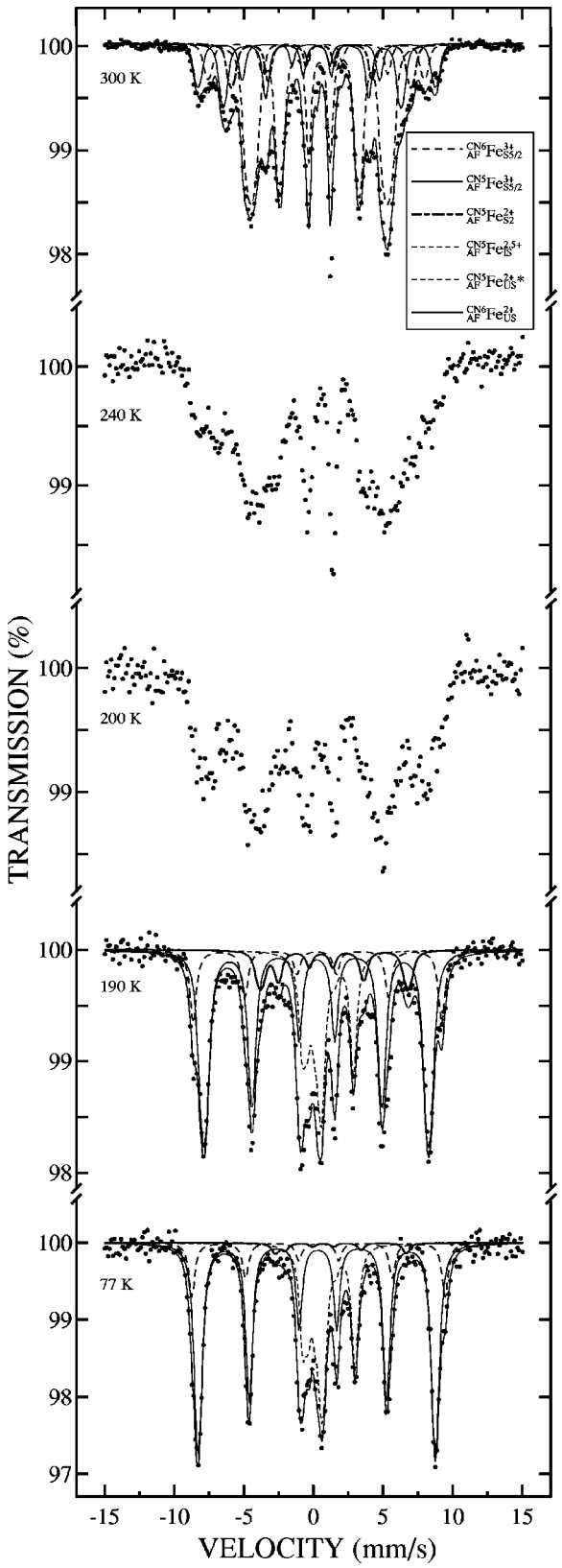

FIG. 14. Mössbauer spectra for $SmBaFe_2O_{5.091}$ at varied temperature.

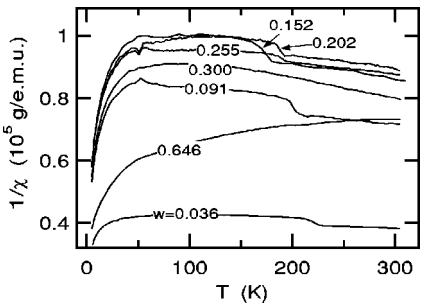

FIG. 15. Inverse magnetic susceptibility vs temperature for selected samples of $SmBaFe_2O_{5+w}$. Measuring points are omitted for clarity.

E. Magnetic and calorimetric measurements

Magnetic susceptibility has been systematically recorded for all samples subjected to this study (Fig. 15). A jump in $1/\chi$ is observed for the samples with $w \leqslant 0.25$ in the temperature range 180–230 K. In the same range, DSC reveals a small endothermic effect upon temperature increase. The evaluated transition temperatures from both techniques give a *u*-shaped dependence on the oxygen content parameter *w*, having a minimum for *w* around 0.15 (Fig. 16, upper part). In the lower part of this illustration, the magnitude of these manifestations is plotted. The transition temperatures thus observed are close both in value and trend to T_V evaluated from Mössbauer temperature scans.

IV. DISCUSSION

The observation of the mixed-valence state in $SmBaFe_2O_{5+w}$ gives rise to a number of closely related questions. The most fundamental of these concern the mechanism which promotes the valence mixing. The first possibility which was considered was that the electron oscillation takes place directly between iron atoms located in oppositely facing square pyramids along the *c* axis, see Fig. 1. This possibility was rejected with the argument that the long Fe–Fe separations along *c* would imply an unlikely electron tunneling process. It was therefore postulated that the electron oscillation process in the involved $Fe^{2+}-Fe^{3+}$ pairs takes place within the *a,b* plane. The next postulate in our

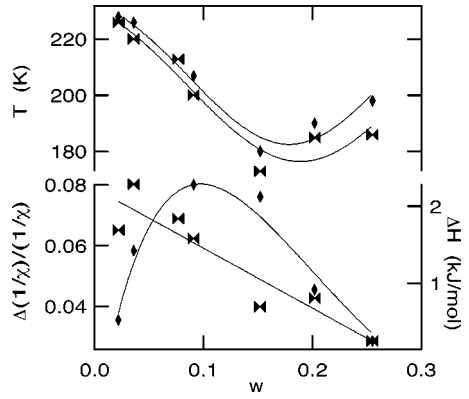

FIG. 16. *Upper part*: Midpoint temperature of magnetic susceptibility anomaly (diamonds) and peak temperature for endothermic DSC effect (bow ties) vs *w* in $SmBaFe_2O_{5+w}$. *Lower part*: The magnitude of these effects.

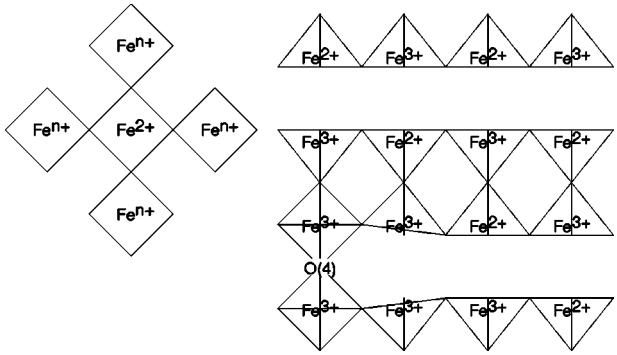

FIG. 17. *Left*: An Fe^{2+} neighborhood in the *a,b* plane (bases of square pyramids) considered for the local probability model for occurrence of the mixed-valence state for Fe^{2+}–Fe^{3+} couples. *Right*: The effect of the added oxygen O(4) on iron valences in neighboring coordinations; view perpendicular to that on the left hand side.

model considerations was to introduce the concept that the oscillation process takes place between an Fe^{2+} in a given square pyramid and Fe^{3+} located on the same *c* level in one of the four nearest-neighbor unit cells. The postulated model situation is sketched in the left part of Fig. 17 showing the basal planes of the square pyramids (see Fig. 1). The Fe^{2+} coordination in the center is surrounded by four Fe^{n+} where *n* can be either 2 or 3.

The key concepts of the postulated electron oscillation process are the following: (i) At least one of the nearest coordination pyramids is populated with Fe^{3+}. (ii) The actual oscillation is conducted via an intermediate oxygen [located at the corner of the square-pyramid base in the left part of Fig. 17, and denoted O(2) or O(3) in Fig. 1]. The implied oscillation process may superficially resemble the superexchange in cooperative magnetism.

In order to establish a measure for the amount of iron participating in the mixed-valence state we have applied a statistical model which assumes random distribution of Fe^{2+} and Fe^{3+}. The objective is to calculate the theoretical amount of $Fe^{2.5+}$ as a function of *w*. The starting point is Fe^{2+} with a molar fraction of $0.5-w$ with respect to iron. In order to form a mixed-valence pair, the central Fe^{2+} (Fig. 17, left) must have at least one Fe^{3+} ion as a nearest neighbor. The probability for this coincidence is $[1-(0.5-w)^4]$. Furthermore, it is assumed that every added oxygen (w) on the average excludes four Fe^{3+} from the pairing process (Fig. 17, right), two in octahedral and two in adjacent square-pyramidal coordinations. The fraction of Fe^{3+} ions which has not become disabled in this manner is $0.5-w$, the overall fraction of Fe^{3+} is $0.5+w$, and hence the probability that a given Fe^{3+} is able to participate in the pairing is $(0.5-w)/(0.5+w)$. The molar fraction of $Fe^{2.5+}$ for a specific value of *w* is then given by the expression

$$x_{MV}(w) = 2(0.5-w)[1-(0.5-w)^4]\frac{0.5-w}{0.5+w}, \qquad (1)$$

where the factor 2 accounts for the fact that there are two Fe per $Fe^{2.5+}$ pair. Figure 18 shows this expression along with the observed Mössbauer intensity for the $Fe^{2.5+}$ component in the 300 K data. The model agrees well with the data and

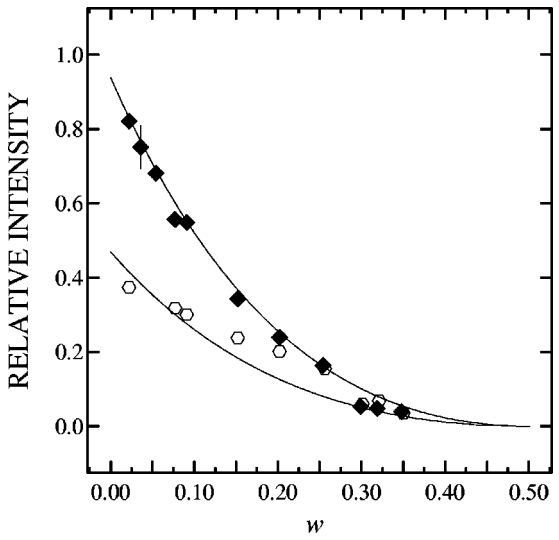

FIG. 18. Experimental and theoretical [curve; Eq. (1)] amount of $^{CN5}_{AF}Fe^{2.5+}_{IS}$ in $SmBaFe_2O_{5+w}$ above T_V (diamonds; 300 K) and its daughter component $^{CN5}_{AF}Fe^{2+}_{US}*$ below T_V (hexagons; 77 K) vs the oxygen content parameter w. Standard deviations that exceed the size of symbols are marked with bars.

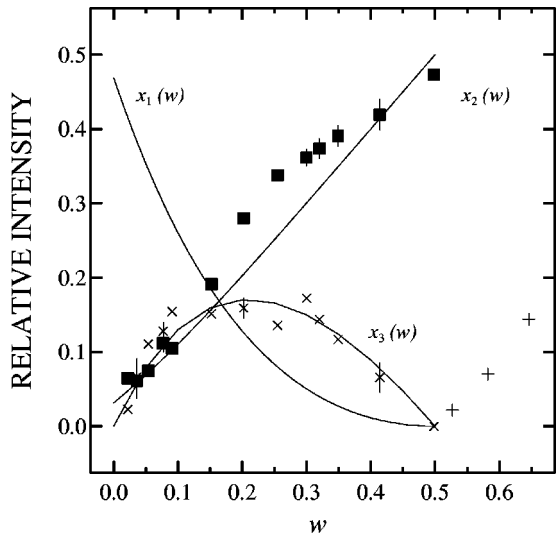

FIG. 19. Intensities of the parent $^{CN5}_{AF}Fe^{3+}_{S5/2}$ component (squares) and its satellite (crosses) compared with the functions specified in Eqs. (2)–(4). (For $w>0.5$ the satellite belongs to $^{CN6}_{AF}Fe^{3+}_{S5/2}$.) Standard deviations that exceed the size of symbols are marked with bars.

predicts in particular that the relative intensity of the mixed-valence component should not reach 1% for $w=0$. The model can also be tested below T_V, where the focus is on the 8 T, $^{CN5}_{AF}Fe^{2+}_{US}*$ component, which should in principle occur with an intensity that is precisely half of that of the mixed-valence state. Figure 18, where $x_{MV}(w)/2$ is plotted together with the relative intensity of $^{CN5}_{AF}Fe^{2+}_{US}*$, shows a reasonable agreement.

The origin of the satellite to $^{CN5}_{AF}Fe^{3+}_{S5/2}$ ($0.0<w<0.5$) can also be accounted for in a corollary to the statistical model for the mixed-valence state. The Fe^{3+} ions in square-pyramidal coordination (overall fraction 0.5 throughout the range $0\leqslant w\leqslant 0.5$) can be divided into three categories:

(i) Those that at the given instant are engaged in mixed-valence pairs. Following Eq. (1), the molar fraction of such ions is

$$x_1(w)=x_{MV}(w)/2. \tag{2}$$

(ii) Those that are configurationally disabled from taking part in the pairing, either owing to the added oxygen (as above; their molar fraction is w), or because they are surrounded by four other Fe^{3+} ions [the probability of which is $(0.5-w)^5$]:

$$x_2(w)=w+(0.5-w)^5. \tag{3}$$

(iii) The rest are those that could potentially participate in mixed-valence pairs but, at the given instant, do not:

$$x_3(w)=0.5-x_1(w)-x_2(w). \tag{4}$$

When these concentrations are plotted as functions of w (Fig. 19), it is seen immediately that the category (ii) corresponds to the parent $^{CN5}_{AF}Fe^{3+}_{S5/2}$ component and the category (iii) corresponds to the satellite. In fact, $x_2(w)$ and $x_3(w)$ account quite well for the observed Mössbauer intensities.

A possible mechanism behind the satellite can again be illustrated with the sketch on the left side of Fig. 17. An Fe^{2+} ion will (except for statistically rare cases) be surrounded by more than one Fe^{3+}. *All these* Fe^{3+} *ions* will be inclined to form a mixed-valence state with the central Fe^{2+} via electron oscillation. However, only one of them will successfully create $Fe^{2.5+}$, whereas the attempted electron oscillations from the other Fe^{3+} ions consequently must be unsuccessful. The unsuccessful attempts [Eq. (4)] of this dynamic process are then assumed to manifest themselves in the satellite to the parent $^{CN5}_{AF}Fe^{3+}_{S5/2}$ component.

It is possible that similar arguments may account for the occurrence of the satellite to $^{CN6}_{AF}Fe^{3+}_{S5/2}$, hence for $w>0.5$ (see Fig. 19).

Another striking feature of the mixed-valence spectra is the distinct dependence of internal magnetic fields on w at 300 K (Fig. 11). In contrast, practically no dependence is seen at 77 K (Fig. 7), when the valences (charges) are separated. The inference is that the variation at 300 K is caused by disordering of the AF moments which originates from the dynamic valence-state mixing. When there is a large fraction of the mixed-valence state, the fraction of unsuccessful attempts is small (see Figs. 18 and 19), the mixed-valence pairs are neatly arranged, and the frustration effect on the AF arrangement is small. When the fraction of the unsuccessful attempts increases, the frustration should also increase. Hence, the maximum in frustration effect manifests itself as a maximum in the satellite intensity (Fig. 18) and a minimum in the internal magnetic field for the mixed-valence component (Fig. 11). The frustration of the internal fields seen for the other components may be considered as an induced, secondary effect of the primary frustration of the mixed-valence state. This would explain why the different internal fields in Fig. 11 show somewhat individual, rather than entirely parallel, composition dependences.

The markedly different behaviors of the internal fields at 77 and 300 K as functions of w (Figs. 7 and 11) are also

reflected in the sudden increase in magnetic susceptibility at the transition to the mixed-valence state (Fig. 15). The magnitude of the susceptibility increase follows the same trend as the product of the molar fractions of the mixed-valence state [Eq. (1)] and the satellite [Eq. (4)]:

$$\frac{\Delta(1/\chi)}{1/\chi} = k[x_{\mathrm{MV}}(w)x_3(w)], \tag{5}$$

where k is a scaling factor. A least squares fit to Eq. (5) has actually been used in the lower part of Fig. 16 to draw the curve [$k=1.1876(6)$]. The good match to the experimental data suggests that the susceptibility increase at T_V corresponds to the perturbation of the AF order in the mixed-valence state caused by frustration from the unsuccessful pairing attempts. The perturbation has a maximum when the number of fluctuations between successful [$x_{\mathrm{MV}}(w)$] and unsuccessful [$x_3(w)$] attempts is largest and the perturbation disappears when either the former or the latter is zero. Hence, the magnetic susceptibility is a single-variable measure of this multivariable magnetic phenomenon.

The transition to the fluctuating mixed-valence state manifests itself as an endothermic effect in DSC (Fig. 16) observed upon heating. This suggests that the transition is driven by an entropy increase ($\Delta H = T\Delta S$). Since the shape of the ΔH vs w relationship correlates with $x_{MV}(w)$, the entropy increase must largely be due to the mixed-valence state formation (Fig. 18), suggesting in turn that a disordering of a low-temperature charge-ordered state may take place. A minor contribution from disordering of the mixed-valence oscillating pairs (fluctuations due to the unsuccessful attempts) may be indicated by the decrease in ΔH for the most reduced sample. In the light of this, the maximum in the calorimetric effect does not have to coincide with that in the magnetic susceptibility.

It should be noted that a likely composition dependence of the electronic oscillation frequency has not been taken into account in any of the the above considerations. This would clearly represent some minor adjustments of the present model, and it is likely that better fits between the experimental data and theoretical predictions in Figs. 18 and 19 could be obtained in a thus modified model.

*Present address: Center for Scientific Computing, 02101 Espoo, Finland.

[1] P. A. Cox, *Transition Metal Oxides* (Clarendon, Oxford, 1992); E. J. W. Verwey and P. W. Haayman, Physica (Amsterdam) **8**, 979 (1941).

[2] M. Campagna, E. Bucher, G. K. Wertheim, D. N. Buchanan, and L. D. Longinotti, Phys. Rev. Lett. **32**, 885 (1974).

[3] E. R. Bauminger, I. Felner, D. Levron (Lebenbaum), I. Nowik, and S. Ofer, Phys. Rev. Lett. **33**, 890 (1974).

[4] T. Penney and F. Holtzberg, Phys. Rev. Lett. **34**, 322 (1975).

[5] Y. Noda, M. Shimada, M. Koizumi, and F. Kanamaru, J. Solid State Chem. **28**, 379 (1979).

[6] K. B. Garg, H. S. Chauhan, U. Chandra, K. S. Jerath, and F. Grandjean, Solid State Commun. **62**, 575 (1987).

[7] M. Takano, N. Nakanishi,, Y. Takeda, S. Naka, and T. Takada, Mater. Res. Bull. **12**, 923 (1977).

[8] L. Fournès, L. Potin, J. C. Grenier, G. Demazeau, and M. Pouchard, Solid State Commun. **62**, 239 (1987).

[9] I. Nowik, I. Felner, and V. P. S. Awana, J. Magn. Magn. Mater. **192**, 67 (1999).

[10] P. Karen and P. M. Woodward, J. Mater. Chem. **9**, 789 (1999).

[11] L. Er-Rakho, C. Michel, Ph. Lacorre, and B. Raveau, J. Solid State Chem. **73**, 531 (1988).

[12] P. Karen and A. Kjekshus, J. Am. Ceram. Soc. **77**, 547 (1994).

[13] I. Barin and O. Knacke, *Thermochemical Properties of Inorganic Substances* (Springer, Berlin, 1973), pp. 316 and 584.

[14] I. Barin, O. Knacke, and O. Kubashevski, *Thermochemical Properties of Inorganic Substances, Supplement* (Springer, Berlin, 1977), p. 295.

[15] P.-E. Werner, The Computer Programme SCANPI 9, Institute of Inorganic Chemistry, University of Stockholm, Sweden, 1992 (unpublished).

[16] R. Blachnik, G. Kudermann, F. Grønvold, A. Alles, B. Falk, and E. F. Westrum, Jr., J. Chem. Thermodyn. **10**, 507 (1978).

[17] N. N. Greenwood and T. C. Gibb, *Mössbauer Spectroscopy* (Chapman and Hall, London, 1971).

[18] M. Nagase, J. Lindén, J. Miettinen, M. Karppinen, and H. Yamauchi, Phys. Rev. B **58**, 3371 (1998).

[19] M. Nagase, J. Lindén, H. Suematsu, M. Karppinen, and H. Yamauchi, Phys. Rev. B **59**, 1377 (1999).

[20] V. Caignaert, I. Mirebeau, F. Bourée, N. Nguyen, A. Ducouret, J.-M. Greneche, and B. Raveau, J. Solid State Chem. **114**, 24 (1995).

[21] A. W. Mombru, C. Christides, A. Lappas, K. Prassides, M. Pissas, C. Mitros, and D. Niarchos, Inorg. Chem. **33**, 1255 (1994).

[22] Q. Huang, P. Karen, V. L. Karen, A. Kjekshus, J. W. Lynn, A. D. Mighell, N. Rosov, and A. Santoro, Phys. Rev. B **45**, 9611 (1992).